

This copy is for your personal, non-commercial use only.

If you wish to distribute this article to others, you can order high-quality copies for your colleagues, clients, or customers by [clicking here](#).

Permission to republish or repurpose articles or portions of articles can be obtained by following the guidelines [here](#).

The following resources related to this article are available online at www.sciencemag.org (this information is current as of March 4, 2010):

Updated information and services, including high-resolution figures, can be found in the online version of this article at:

<http://www.sciencemag.org/cgi/content/full/327/5970/1258>

Supporting Online Material can be found at:

<http://www.sciencemag.org/cgi/content/full/327/5970/1258/DC1>

This article **cites 18 articles**, 8 of which can be accessed for free:

<http://www.sciencemag.org/cgi/content/full/327/5970/1258#otherarticles>

This article appears in the following **subject collections**:

Microbiology

<http://www.sciencemag.org/cgi/collection/microbio>

number and distribution by the condensin I complex (3) and execution of NCOs by RTEL-1.

References and Notes

- K. J. Hillers, A. M. Villeneuve, *Curr. Biol.* **13**, 1641 (2003).
- W. Wood, *The Nematode Caenorhabditis elegans* (Cold Spring Harbor Laboratory Press, Cold Spring Harbor, NY, 1988).
- D. G. Mets, B. J. Meyer, *Cell* **139**, 73 (2009).
- L. J. Barber *et al.*, *Cell* **135**, 261 (2008).
- Materials and methods are available as supporting material on *Science* Online.
- P. M. Meneely, A. F. Farago, T. M. Kauffman, *Genetics* **162**, 1169 (2002).
- C. J. Tsai *et al.*, *Genes Dev.* **22**, 194 (2008).
- B. O. Krogh, L. S. Symington, *Annu. Rev. Genet.* **38**, 233 (2004).
- E. Martini, R. L. Diaz, N. Hunter, S. Keeney, *Cell* **126**, 285 (2006).
- S. Y. Chen *et al.*, *Dev. Cell* **15**, 401 (2008).
- N. Bhalla, D. J. Wynne, V. Jantsch, A. F. Dernburg, R. S. Hawley, *PLoS Genet.* **4**, e1000235 (2008).
- D. K. Bishop, D. Zickler, *Cell* **117**, 9 (2004).
- N. M. Hollingsworth, S. J. Brill, *Genes Dev.* **18**, 117 (2004).
- T. Garcia-Muse, S. J. Boulton, *Chromosome Res.* **15**, 607 (2007).
- M. Zetka, *Genome Dyn.* **5**, 43 (2009).
- M. S. McMahonill, C. W. Sham, D. K. Bishop, *PLoS Biol.* **5**, e299 (2007).

- M. P. Colaiácovo *et al.*, *Dev. Cell* **5**, 463 (2003).
- This work was supported by Cancer Research UK (S.J.B. and S.C.W.) and the Canadian Institute of Health Research (A.M.R.). B.J.M. is an investigator of the Howard Hughes Medical Institute.

Supporting Online Material

www.sciencemag.org/cgi/content/full/327/5970/1254/DC1
Materials and Methods
SOM Text
Figs. S1 to S7
Tables S1 and S2
References

9 October 2009; accepted 28 January 2010
10.1126/science.1183112

Spatially Ordered Dynamics of the Bacterial Carbon Fixation Machinery

David F. Savage,* Bruno Afonso,* Anna H. Chen, Pamela A. Silver†

Cyanobacterial carbon fixation is a major component of the global carbon cycle. This process requires the carboxysome, an organelle-like proteinaceous microcompartment that sequesters the enzymes of carbon fixation from the cytoplasm. Here, fluorescently tagged carboxysomes were found to be spatially ordered in a linear fashion. As a consequence, cells undergoing division evenly segregated carboxysomes in a nonrandom process. Mutation of the cytoskeletal protein ParA specifically disrupted carboxysome order, promoted random carboxysome segregation during cell division, and impaired carbon fixation after disparate partitioning. Thus, cyanobacteria use the cytoskeleton to control the spatial arrangement of carboxysomes and to optimize the metabolic process of carbon fixation.

Efficient cellular metabolism relies on the compartmentalization of enzymatic reactions. Prokaryotes achieve this organization by using capsidlike protein microcompartments to isolate metabolic pathways from the cellular milieu (1–3). The best-characterized microcompartment, the carboxysome, is found in cyanobacteria and chemoautotrophs and is responsible for catalyzing

more than 40% of Earth's carbon fixation (2, 4). Structurally, the carboxysome consists of an icosahedral proteinaceous shell that encloses the enzymes carbonic anhydrase and ribulose-1,5-bisphosphate carboxylase-oxygenase (RuBisCO) (5–8). The shell may act as a semipermeable barrier, allowing the passive import of the negatively charged reactants, HCO_3^- and ribulose 1,5-bisphosphate, and excluding the competing substrate O_2 . Within the carboxysome, carbonic anhydrase catalyzes the production of CO_2 , where it is fixed by RuBisCO into 3-phosphoglycerate. Carbon fixation is the basis of biosynthesis in cyanobacteria, and genetic disruption of the car-

boxysome is lethal (9, 10). Thus, the proper assembly and function of carboxysomes is fundamental to carbon fixation and cellular fitness.

We developed methods to visualize carboxysomes and to investigate their dynamical behavior in living cells. The carboxysome consists of ~5000 monomers of the shell protein CcmK and ~2000 monomers of RuBisCO (5). Expression of these proteins in the cyanobacterium *Synechococcus elongatus* PCC7942 (hereafter *Synechococcus*) (11) fused to green, yellow, or cyan fluorescent protein (GFP, YFP, or CFP) yielded fluorescent particles, and the proteins colocalized when coexpressed in the same cell, which indicated assembled carboxysomes (Fig. 1A). The labeled carboxysomes also contained endogenous RuBisCO (Fig. 1B). Electron microscopy showed that all carboxysomes contain RbcL-GFP and that all RbcL-GFP was in carboxysomes (Fig. 1C). Carboxysome morphology and cellular growth rates were unaffected by YFP fusions (fig. S1).

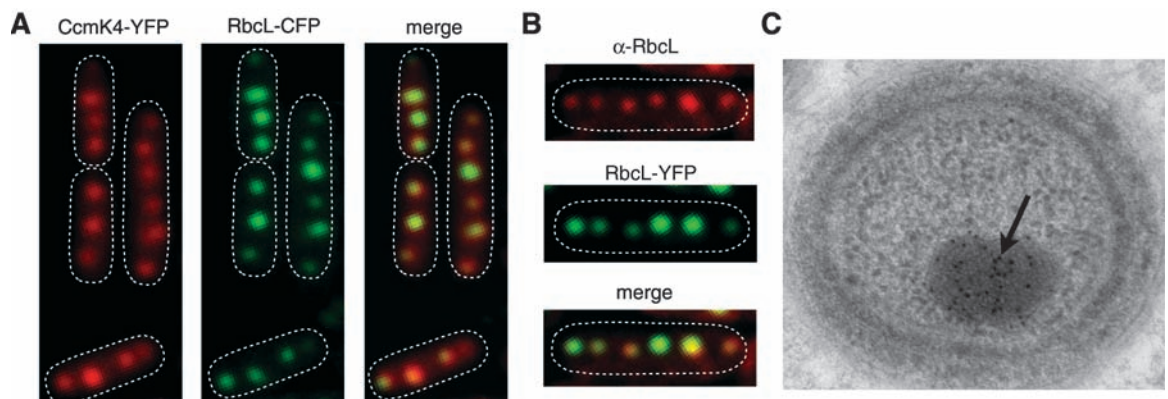
Carboxysomes were evenly spaced along the long axis of *Synechococcus* (Fig. 2A). On average, there were 3.7 ± 1.2 carboxysomes per cell under log phase growth (Fig. 2B). We calculated the pairwise distances between carboxysomes in cells ($n = 2508$) with four carboxysomes (Fig. 2C). The average spacing between adjacent carboxysomes was $0.66 \mu\text{m}$ but was proportional to cell length (Fig. 2D). Thus, normalizing by cell length sharpened the pair-

Department of Systems Biology, Harvard Medical School, Boston, MA 02115, USA.

*These authors contributed equally to this work.

†To whom correspondence should be addressed. E-mail: pamelasilver@hms.harvard.edu

Fig. 1. The carboxysome can be fluorescently labeled. (A) Fluorescence colocalization of shell protein CcmK4-YFP and RuBisCO protein RbcL-CFP. (B) Immunofluorescence microscopy with an antibody against RuBisCO as a probe and showing RbcL-YFP colocalized to cytoplasmic RuBisCO. (C) Transverse cell electron micrograph showing, by means of immunogold labeling with an antibody against GFP, localization of RbcL-GFP to carboxysomes.



wise distance probability distribution (Fig. 2E). This suggested that the spacing of carboxysomes could be actively controlled.

The diffusive dynamics of individual carboxysomes over time was constrained (Fig. 3A). Carboxysomes ($n = 350$) had an average diffusion coefficient D of $4.58 \times 10^{-5} \pm 4.50 \times 10^{-5} \mu\text{m}^2/\text{s}$

(Fig. 3A). Using cytoplasmic parameters (12) and a mean particle radius of 50 nm, we estimate a theoretical value of $D = 3.85 \times 10^{-1} \mu\text{m}^2/\text{s}$, four orders of magnitude greater than the observed. The measured value of D suggests that a carboxysome will diffuse an average distance $r = [4 \times 4.58 \times 10^{-5} \mu\text{m}^2/\text{s} \times 64,800 \text{ s}]^{1/2} = 3.45 \mu\text{m}$

during the cell cycle. Considering the displacement occurring from cell growth, the carboxysomes do not appear to be diffusing randomly.

Carboxysomes are known to associate with cellular structures, including unidentified filaments (1, 13, 14). Deletions of the five (*mreB*,

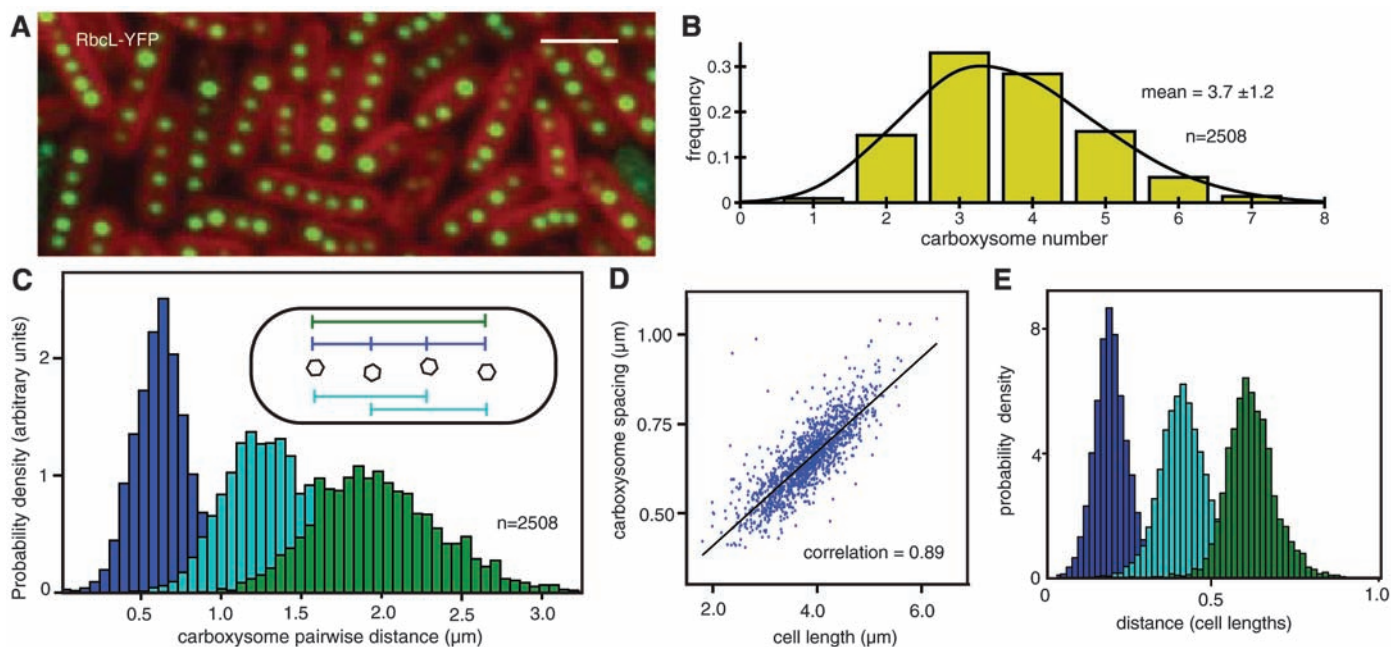
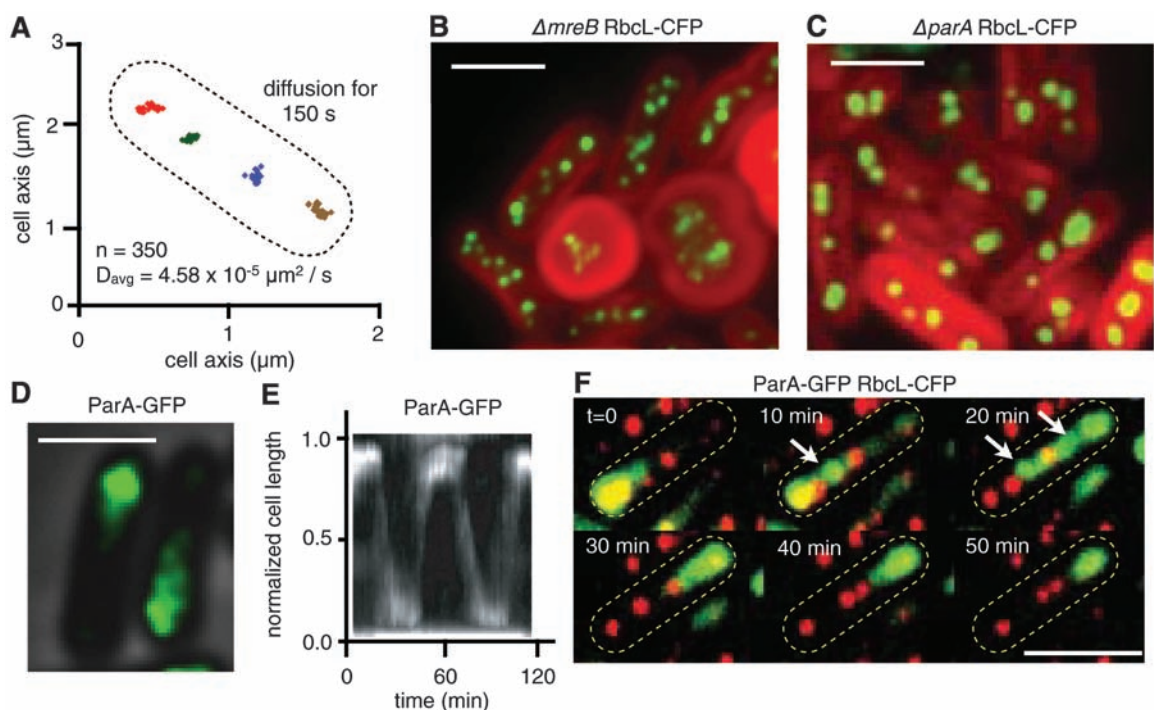


Fig. 2. Carboxysomes are spatially organized in vivo. (A) RbcL-YFP (green) expression shows organized carboxysomes. Thylakoid membrane fluorescence is shown in red. (B) Average number of carboxysomes per cell. (C) Pairwise

distance between carboxysomes in cells with four carboxysomes. (D) Carboxysome spacing is proportional to cell length. (E) Same as (C) except carboxysome distances were normalized for cell length.

Fig. 3. Carboxysomes are organized by the cytoskeleton. (A) Diffusion of four tracked carboxysomes. Trajectories were used to compute D in the two-dimensional diffusion equation $\langle r^2 \rangle = 4Dt$, where t is time. (B) RbcL-CFP (green) in *mreB*-deficient cells showing spherical cells and loss of carboxysome spatial organization. Thylakoid membrane fluorescence is shown in red. (C) RbcL-CFP (green) in $\Delta\textit{parA}$ cells showing the loss of carboxysome spatial organization with no change in morphology. (D) Fluorescence image of ParA-GFP overlaid onto phase-microscopy image of cells showing the filament-like nature of ParA. Image is the deconvolved middle focal plane of a z stack. (E) Kymograph of the oscillatory behavior of ParA-GFP showing polymer dynamics. (F) ParA oscillation in relation to carboxysomes. Arrows denote increased ParA-GFP (green) between carboxysomes (RbcL-CFP, red). Scale bars, 2 μm .



deconvolved middle focal plane of a z stack. (E) Kymograph of the oscillatory behavior of ParA-GFP showing polymer dynamics. (F) ParA oscillation in relation to carboxysomes. Arrows denote increased ParA-GFP (green) between carboxysomes (RbcL-CFP, red). Scale bars, 2 μm .

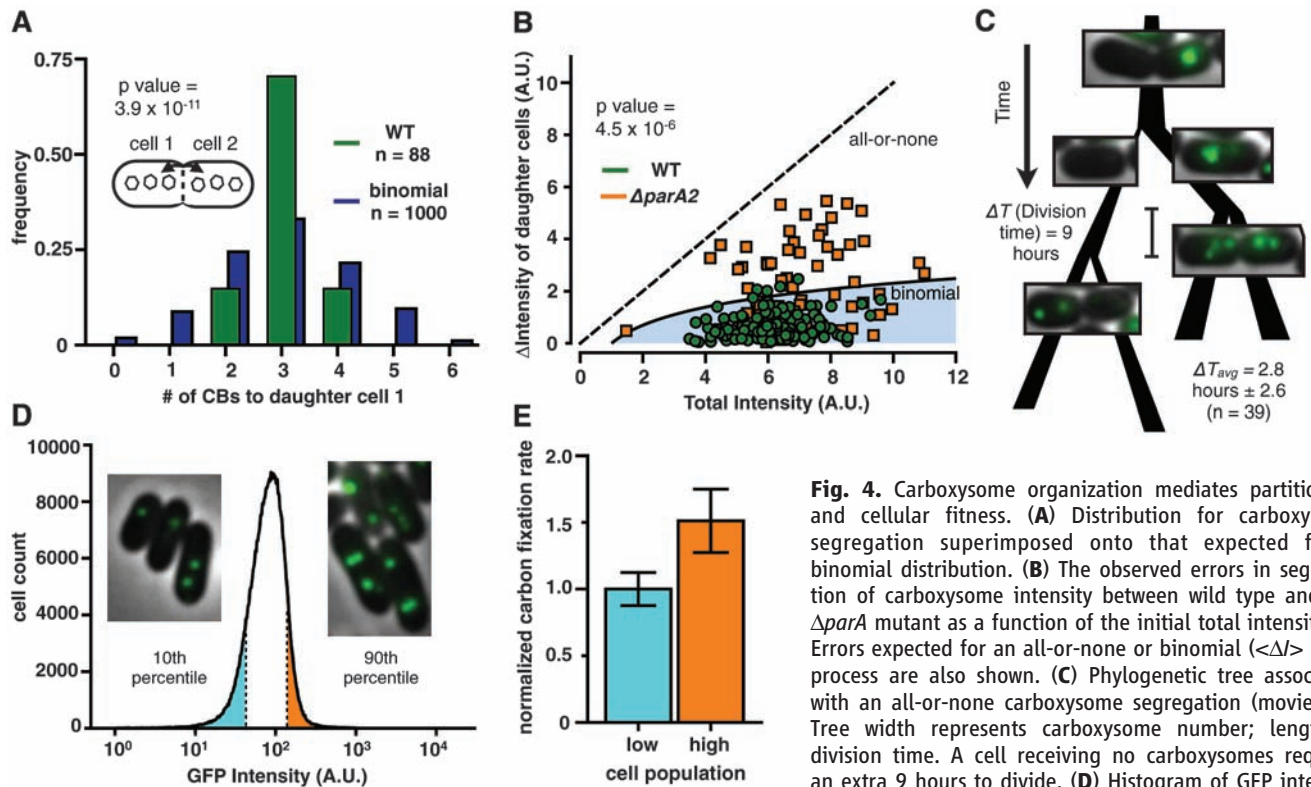


Fig. 4. Carboxysome organization mediates partitioning and cellular fitness. **(A)** Distribution for carboxysome segregation superimposed onto that expected for a binomial distribution. **(B)** The observed errors in segregation of carboxysome intensity between wild type and the $\Delta parA$ mutant as a function of the initial total intensity (I). Errors expected for an all-or-none or binomial ($\langle \Delta I \rangle \approx \sqrt{I}$) process are also shown. **(C)** Phylogenetic tree associated with an all-or-none carboxysome segregation (movie S3). Tree width represents carboxysome number; length is division time. A cell receiving no carboxysomes requires an extra 9 hours to divide. **(D)** Histogram of GFP intensity in $\Delta parA$ cells expressing RbL-GFP. The upper (orange)

and lower (cyan) 10% of intensities were sorted and verified by microscopy (inset). **(E)** ^{14}C carbon fixation rates (with standard deviation, $n = 3$) of the populations sorted in **(D)**. The populations are different as judged by an unpaired t test ($P = 2.9 \times 10^{-2}$).

ftsZ, *minD*, and two *parA*-like genes) annotated cytoskeletal genes present in the *Synechococcus* genome were constructed (11). Mutations in *mreB* and the *parA*-like gene *Synpcc7942_1833* (hereafter, *parA*) disrupted carboxysome organization (Fig. 3, B and C). As deletion of *mreB* was pleiotropic, we investigated *parA* (15).

Deletion of *parA* showed disruption of carboxysome order with no perturbation of cellular morphology (Fig. 3C). ParA-GFP formed filament-like structures at one pole (Fig. 3D), that depolymerized and reassembled at the opposite pole in an oscillatory manner (period of 33.3 ± 10.6 min, $n = 25$) consistent with other ParA proteins (16) (Fig. 3E and movie S1). During oscillations, the filament frequently (68%, $n = 40$) hesitated or left a trail of condensed polymer behind the ParA wavefront. In the latter case, the polymer dissipated but reappeared in the same location after another oscillation. This condensed polymer was found between carboxysomes, which suggested that ParA mediates the connections between adjacent carboxysomes (Fig. 3F and movie S2).

Carboxysomes are essential for carbon fixation, so their organization may function to ensure even segregation during cell division. *Synechococcus* were entrained using a diurnal cycle of light, such that cells divided in synchrony. Single cells were tracked by using phase-contrast microscopy, and fluorescent images of labeled carboxysomes were acquired over several cell

cycles. Each daughter cell consistently received an equal number of carboxysomes during division (Fig. 4A). Cytoplasmic proteins are thought to partition randomly (17), but segregation of carboxysomes was highly nonrandom (Pearson's chi-square test, $P = 3.9 \times 10^{-11}$). Because of the loss of equal spacing, resolving individual carboxysomes was not possible; instead, we quantified the intensity of carboxysomes partitioning to daughter cells. The *parA* deletion strain exhibited much lower fidelity in partitioning carboxysomes than did wild-type cells (two-tailed Kolmogorov-Smirnov test, $P = 4.4 \times 10^{-6}$) (Fig. 4B).

The loss of carboxysome organization was responsible for reduced fitness. We observed divisions in which one $\Delta parA$ daughter cell received no carboxysomes. Lineage tracking revealed that these cells divided 2.8 ± 2.6 ($n = 39$) hours later than their corresponding sister cells (Fig. 4C and movies S3 to S5). Populations of newly divided $\Delta parA$ cells with low or high numbers of carboxysomes were isolated by cell sorting (Fig. 4D). Cells with more carboxysomes fixed $\sim 50\%$ more carbon per unit of time than cells with fewer did (Fig. 4E). Thus, disruption of carboxysome spatial organization compromised the fidelity of carboxysome partitioning and impaired daughter-cell fitness.

The regular spacing of cellular machinery is emerging as a fundamental aspect of bacterial physiology. Vesicular magnetosomes and plas-

mids distribute regularly along the long axis of the cell (16, 18). Here, an enzymatic complex was observed to behave in a similar manner. The organization of carboxysomes depends on cytoskeletal components, including ParA and MreB. Because MreB is located underneath the inner membrane (19), we favor a model in which MreB defines a structure that is used to organize carboxysomes. ParA proteins evenly space plasmids in the cell and mediate the positioning of a pole-localized protein in *Rhodobacter sphaeroides* (20). Here, mutation of *parA* affected carboxysome organization, and ParA filaments connected adjacent carboxysomes. Thus, ParA is a specific mediator of carboxysome spacing.

Carboxysomes occur in small numbers such that noise fluctuations during cell division could yield a daughter cell without this essential metabolic complex. It is thus possible that evolutionary pressures have selected for an organizational system—similar to nucleic acid sorting and perhaps derived from it—that ensures that each daughter cell receives a sufficient number of carboxysomes to optimize carbon fixation and cellular fitness.

References and Notes

1. J. M. Shively, F. L. Ball, B. W. Kline, *J. Bacteriol.* **116**, 1405 (1973).
2. G. C. Cannon *et al.*, *Appl. Environ. Microbiol.* **67**, 5351 (2001).
3. T. O. Yeates, C. A. Kerfeld, S. Heinhorst, G. C. Cannon, J. M. Shively, *Nat. Rev. Microbiol.* **6**, 681 (2008).

4. J. Overmann, F. Garcia-Pichel, in *The Prokaryotes*, vol. 2, *Ecophysiology and Biochemistry*, M. Dworkin et al., Eds. (Springer, New York, 2006), pp. 32–85.
 5. C. V. Iancu et al., *J. Mol. Biol.* **372**, 764 (2007).
 6. M. F. Schmid et al., *J. Mol. Biol.* **364**, 526 (2006).
 7. C. A. Kerfeld et al., *Science* **309**, 936 (2005).
 8. S. Tanaka et al., *Science* **319**, 1083 (2008).
 9. H. Ohkawa, M. Sonoda, H. Katoh, T. Ogawa, *Can. J. Bot.* **76**, 1035 (1998).
 10. G. D. Price, S. M. Howitt, K. Harrison, M. R. Badger, *J. Bacteriol.* **175**, 2871 (1993).
 11. Materials and methods are available as supporting material on Science Online.
 12. M. B. Elowitz, M. G. Surette, P. E. Wolf, J. B. Stock, S. Leibler, *J. Bacteriol.* **181**, 197 (1999).
 13. T. E. Jensen, R. P. Ayala, *Arch. Microbiol.* **111**, 1 (1976).
 14. C. V. Iancu et al., *J. Mol. Biol.* **396**, 105 (2010).
 15. M. Thanbichler, L. Shapiro, *Nat. Rev. Microbiol.* **6**, 28 (2008).
 16. G. Ebersbach, K. Gerdes, *Annu. Rev. Genet.* **39**, 453 (2005).
 17. N. Rosenfeld, J. W. Young, U. Alon, P. S. Swain, M. B. Elowitz, *Science* **307**, 1962 (2005).
 18. A. Komeili, *Annu. Rev. Biochem.* **76**, 351 (2007).
 19. H. J. Defeu Soufo, P. L. Graumann, *BMC Cell Biol.* **6**, 10 (2005).
 20. S. R. Thompson, G. H. Wadhams, J. P. Armitage, *Proc. Natl. Acad. Sci. U.S.A.* **103**, 8209 (2006).
 23. We thank R. Milo, R. Ward, R. Losick, S. Stanley, and E. Garner for comments on the manuscript; M. Ericsson and L. Benecchi for electron microscopy; and S. Golden for reagents. D.F.S. is a U.S. Department of Energy Biosciences Fellow of the Life Sciences Research Foundation. B.A. is supported by the Fundação para a

Ciência e a Tecnologia and Graduate Program in Areas of Basic and Applied Biology (GABBA). This work was supported by Army Research Office Award W911NF-09-1-0226.

Supporting Online Material

www.sciencemag.org/cgi/content/full/327/5970/1258/DC1
 Materials and Methods
 SOM Text
 Figs. S1 to S4
 Tables S1 to S3
 References
 Movies S1 to S5

17 December 2009; accepted 22 January 2010
 10.1126/science.1186090

Retromer Is Required for Apoptotic Cell Clearance by Phagocytic Receptor Recycling

Didi Chen,^{1,2*} Hui Xiao,^{1,2*} Kai Zhang,³ Bin Wang,³ Zhiyang Gao,¹ Youli Jian,¹ Xiaying Qi,¹ Jianwei Sun,^{1,2} Long Miao,³ Chonglin Yang^{1†}

The cell surface receptor CED-1 mediates apoptotic cell recognition by phagocytic cells, enabling cell corpse clearance in *Caenorhabditis elegans*. Here, we found that the *C. elegans* intracellular protein sorting complex, retromer, was required for cell corpse clearance by mediating the recycling of CED-1. Retromer was recruited to the surfaces of phagosomes containing cell corpses, and its loss of function caused defective cell corpse removal. The retromer probably acted through direct interaction with CED-1 in the cell corpse recognition pathway. In the absence of retromer function, CED-1 associated with lysosomes and failed to recycle from phagosomes and cytosol to the plasma membrane. Thus, retromer is an essential mediator of apoptotic cell clearance by regulating phagocytic receptor(s) during cell corpse engulfment.

In *Caenorhabditis elegans*, cell corpse engulfment is controlled by two parallel pathways, one that recognizes and transduces engulfing signals, and the other that induces

cytoskeleton reorganization (1). However, how components of these pathways are regulated and what other factors are involved remain unclear. To identify additional regulators of

these pathways we performed genome-wide and candidate-based RNA interference (RNAi) screens (2) for genes whose inactivation greatly increased cell corpse numbers in the *C. elegans* germ line. Three genes, *snx-1*, *snx-6*, and *lst-4*, encoding homologs of mammalian sorting nexins 1/2, 5/6, and 9/18/33, respectively, were identified (figs. S1A and S2A and table S1). In mammals, sorting nexins 1/2 and 5/6 are essential components of the intracellular protein sorting complex retromer (3–5), whereas sorting nexins 9/18/33 regulate endocytosis (3). The deletion mutants *snx-1(tm847)* (6) and *snx-*

¹Key Laboratory of Molecular and Developmental Biology, Institute of Genetics and Developmental Biology, Chinese Academy of Sciences, Datun Road, Chaoyang District, Beijing 100101, China. ²Graduate School, Chinese Academy of Sciences, Beijing 100039, China. ³National Laboratory of Biomacromolecules, Institute of Biophysics, Chinese Academy of Sciences, Datun Road, Chaoyang District, Beijing 100101, China.

*These authors contributed equally to this work.
 †To whom correspondence should be addressed. E-mail: clyang@genetics.ac.cn

Fig. 1. *C. elegans* retromer affects clearance of apoptotic cells. **(A)** Quantification of germ cell corpses in N2 (wild type), *snx-1(tm847)*, *snx-6(tm3790)*, and *snx-6(tm3790);snx-1(tm847)* mutants. **(B)** Four-dimensional microscopy analysis of germ cell corpse duration in N2, *snx-1(tm847)*, and *snx-6(tm3790)* mutants. Thirty germ cell corpses were recorded for each strain. **(C)** Quantification of germ cell corpses in *vps-26(RNAi)*, *vps-35(hu68)*, and *vps-29(tm1320)* animals. **(D)** Germ cell corpse phenotypes of control RNAi- and *vps-29* RNAi-treated N2 and *snx-1(tm847)* mutants. In (A), (C), and (D), the y axis indicates the average number of germ cell corpses. Error bars represent the SEM. Comparisons were performed using unpaired *t* tests. ***P* < 0.001.

